American Mineralogist, Volume 85, pages 473–479, 2000

Raman spectroscopic characteristics of Mg-Fe-Ca pyroxenes

E. HUANG,* C.H. CHEN, T. HUANG, E.H. LIN, AND JI-AN XU

Institute of Earth sciences, Academia Sinica, Taipei 115, Taiwan

ABSTRACT

Raman spectra of several compositions of (Mg, Fe, Ca)SiO_3 pyroxenes were collected at ambient conditions. More than 10 Raman vibrational modes were observed for these pyroxenes in the wavenumber range between 200 and 1200 cm^{-1}. In general, these pyroxenes are characterized by (1) the Si-O stretching modes above 800 cm^{-1}; (2) the Si-O bending modes between 500 and 760 cm^{-1}; (3) SiO_4 rotation and metal-oxygen translation modes below 500 cm^{-1}. For a constant Ca content, frequencies of the Raman modes in the enstatite-ferrosilite (opx) and diopside-hedenbergite (cpx) series generally decrease with an increase in Fe content. This phenomenon is attributed to an increase in both the bonding lengths and the reduced mass as Fe^{2+} is substituted for Mg. However, two modes at ~900 cm^{-1} in the enstatite-ferrosilite series increase in frequencies as Fe content increases. A possible explanation is to the shortening in the Si-O-Si bridging bonding bonds when the M2 sites are preferentially occupied by the iron cation. The effect of Fe substituting for Mg on the frequency shift in cpx is less profound than opx because the larger M2 was occupied by calcium and the substitution of iron and magnesium in the M1 site results in a less significant change in the bond length. The major-element composition of the (Mg, Fe, Ca)-pyroxenes, especially the orthopyroxene series, can be semi-quantitatively determined on the basis of the peak positions of their characteristic Raman modes.

INTRODUCTION

Spectroscopic methods have become a vital investigative tool in determinative mineralogy (Calas and Hawthorne 1988). The infrared (IR) absorption and Raman scattering methods probe the lattice vibrations of a material. Applications of these techniques to the study of rock-forming minerals, which enables us to understand the lattice dynamics of minerals (e.g., McMillan and Hofmeister 1985) and for the calculation of the thermodynamic parameters of the minerals (e.g., Kieffer 1985; Xu et al. 1995).

Minerals of the pyroxene group ($MSiO_3$, where M are cations such as Mg, Ca, Fe^{2+}) are one of the most abundant rock-forming minerals on Earth (Deer et al. 1966). Raman spectroscopic studies on pyroxenes are relatively few (McMillan and Hofmeister 1988) and most are limited to end-member compositions (e.g., White 1975; Mao et al. 1987; Ghose et al. 1994; Hugh Jones et al. 1998; Wang et al. 1994; Chopelas 1999). Here, we report a systematic survey on the Raman spectra of (Mg, Fe, Ca)-bearing pyroxenes over a wide range of composition. The results are used to infer and interpret the possible bonding characters in these minerals. Moreover, the feasibility of using Raman spectroscopy as an indicator of chemical composition of pyroxenes is discussed.

EXPERIMENTAL METHODS

Chemical compositions of all natural single-crystals of pyroxene (Table 1) were analyzed by the electron microprobe. In each sample, several different spots were analyzed to check the homogeneity of the sample. We also examined series of synthetic orthopyroxene with compositions ($En_{97.5}$, En_{80}, En_{75}, En_{70}, En_{60}, En_{50}, En_{40}, En_{35}, En_{30}, En_{25}, En_{17}, and En_{10}) that were produced by H. Yang. See Yang and Ghose (1994) for details. The chemical composition of all the specimens in this study is plotted in Ca-Mg-Fe pyroxene diagram (Fig. 1). Strictly speaking, wollastonite is not a pyroxene. However, it is also included in this study because it is one of the end-members in the $MgSiO_3$-$FeSiO_3$-$CaSiO_3$ composition diagram.

Raman spectra were excited using the 514 nm line of an Argon-Ion laser. We used a Raman spectrometer of the Renishaw Company, which contains a micro-objective that focuses the size of the laser beam to about 5 μm at the surface of the sample. A charge-coupled device is used as a detector to collect the signal in an 180° geometry. The position of the Raman peaks was determined by the PeakFit program. Typical acquisition time was about 10 minutes. Normally, the intensity of the modes varies with the orientation of the single crystal under investigation whereas the wavenumber of the modes remains the same. Therefore, in each sample, several orientations are attempted and an average in the peak position was taken for each vibrational mode. The spectral resolution for each mode is on the order of ±1 cm^{-1}.

*E-mail: eugene@earth.sinica.edu.tw

0003-004X/00/0304–473$05.00

TABLE 1. Chemical composition of natural pyroxene specimens

No.	Mineral	Source	SiO_2	FeO	MgO	CaO	Al_2O_3	Na_2O	MnO	TiO_2	Cr_2O_3	Total
1	Enstatite	Bamble	57.84	6.66	34.84	0.25	0.39	0.01	0.12	——	——	100.11
2	Enstatite	Bamble	56.73	8.76	33.12	0.26	0.09	0.05	0.10	0.05	0.00	99.15
3	Enstatite	St. Ludger-de-Milo	54.06	13.35	29.35	0.24	3.78	0.01	0.27	0.06	0.10	101.22
4	Enstatite	Sh. John Lake	52.60	14.24	28.08	0.20	3.68	0.00	0.19	0.05	0.12	99.16
5	Enstatite	Tsune Cho	54.22	16.82	26.23	1.31	1.49	0.03	0.43	0.30	0.04	100.87
7	Enstatite	Ekersund	50.56	26.97	18.01	2.02	1.17	0.05	0.42	0.19	0.04	99.43
8	Augite	Hualalai	49.37	5.89	16.24	21.80	5.34	0.43	——	0.65	0.61	100.33
10	Augite	Ney Mineral Co.	54.47	15.46	15.39	12.01	1.64	0.39	0.08	0.04	0.03	99.51
11	Augite	Ney Mineral Co.	53.99	16.83	14.38	12.50	1.80	0.52	0.14	0.06	0.00	100.22
13	Diopside	Natural Bridge	54.87	0.24	18.30	25.63	0.11	0.34	0.04	——	——	99.53
14	Diopside	Birds Creek	55.11	0.82	17.89	25.06	0.09	0.06	0.05	0.21	0.00	99.29
15	Diopside	Templeton	53.69	2.83	15.94	24.72	2.11	0.70	0.14	0.10	0.00	100.23
16	Diopside	Pierrepout	54.08	5.31	14.48	23.97	1.18	1.10	0.21	0.05	0.03	100.40
17	Diopside	Otter Lake District	52.34	10.01	11.65	23.64	0.86	0.82	0.27	0.01	0.01	99.61
18	Hedenbergite	Obira mite	50.20	22.56	2.98	23.42	0.24	0.05	1.02	0.02	0.01	100.50
19	Wollastonite	Willsboro	51.44	0.00	0.04	48.83	0.02	0.03	0.01	0.03	0.01	100.41

* Chen et al. (1992).
† Jarosewich et al. (1980).

TABLE 2. The Raman active vibrational modes of the pyroxene in this study

Composition	ν_1	ν_2	ν_2'	ν_3	ν_3'	ν_4	ν_5	ν_6	ν_7	ν_8	ν_9	ν_{10}	ν_{11}	ν_{12}
$En_{.975}Fs_{.025}$	239	–	304	343	–	402	421	446	523	541	552	583	663	686
$En_{.80}Fs_{.20}$	233	–	–	335	–	396	412	–	518	538	–	573	658	678
$En_{.75}Fs_{.30}$	230	–	–	333	–	392	408	–	516	537	–	570	656	676
$En_{.70}Fs_{.40}$	229	–	–	331	–	390	406	–	515	536	–	566	655	675
$En_{.60}Fs_{.50}$	–	–	–	327	–	383	–	–	511	533	–	562	652	671
$En_{.50}Fs_{.60}$	–	–	–	325	–	380	–	416	511	531	–	558	649	669
$En_{.40}Fs_{.65}$	–	–	–	319	–	370	–	406	508	528	–	554	645	665
$En_{.35}Fs_{.70}$	–	–	–	320	–	372	–	406	508	528	–	553	645	665
$En_{.30}Fs_{.75}$	–	–	–	315	–	365	–	405	506	526	–	550	642	663
$En_{.25}Fs_{.83}$	–	–	–	313	–	360	–	400	504	524	–	548	640	661
$En_{.17}Fs_{.83}$	–	–	–	312	–	356	–	395	502	523	–	547	637	660
$En_{.10}Fs_{.90}$	–	–	–	305	–	349	–	392	502	519	–	537	633	657
$^{\#1}En_{.90}Fs_{.10}$	235	–	297	341	–	400	–	441	521	537	549	–	662	683
$^{\#2}En_{.87}Fs_{.13}$	234	–	297	339	–	398	–	439	518	537	548	–	661	682
$^{\#3}En_{.80}Fs_{.20}$	231	–	295	338	–	397	–	437	515	534	543	–	657	680
$^{\#4}En_{.78}Fs_{.22}$	231	–	295	337	–	395	–	437	513	537	544	–	656	680
$^{\#5}En_{.72}Fs_{.26}Wo_{.03}$	230	–	291	335	–	394	–	436	515	533	545	–	657	670
$^{\#7}En_{.52}Fs_{.44}Wo_{.04}$	224	–	292	330	–	386	–	420	513	530	539	–	653	672
$^{\#10}En_{.47}Fs_{.27}Wo_{.26}$	218	–	290	–	357	382	427	–	–	527	558	–	665	–
$^{\#11}En_{.44}Fs_{.29}Wo_{.27}$	218	–	289	–	359	383	424	–	–	525	553	–	667	–
$^{\#13}En_{.50}Wo_{.50}$	230	255	–	325	359	391	–	–	–	–	558	–	665	–
$^{\#14}En_{.49}Fs_{.01}Wo_{.50}$	230	255	–	325	360	392	–	–	508	528	559	–	665	–
$^{\#15}En_{.45}Fs_{.04}Wo_{.50}$	230	255	–	325	359	392	–	–	509	529	558	–	665	–
$^{\#16}En_{.42}Fs_{.08}Wo_{.50}$	229	253	–	325	359	392	–	–	508	528	559	–	664	–
$^{\#17}En_{.34}Fs_{.16}Wo_{.50}$	232	251	–	321	354	386	–	–	505	529	557	–	663	–
$^{\#18}En_{.09}Fs_{.39}Wo_{.52}$	233	–	–	307	338	375	404	–	495	522	549	–	660	–
$^{\#8}En_{.46}Fs_{.09}Wo_{.44}$	–	–	–	323	352	387	–	461*	508	531	556	–	662	–
$^{\#19}Wo$	226*,237	257*	303	321*,337	–	400	412	–	485*	–	–	581	636	688

RESULTS

More than ten Raman vibrational modes were observed in these pyroxenes in the wavenumber range between 200 and 1200 cm^{-1}. (This number is far less than the expected number of modes, see below.) The pyroxenes analyzed are classified as five groups as (1) synthetic orthopyroxene (opx, enstatite-ferrosilite series); (2) natural orthopyroxene; (3) clinopyroxene (cpx, diopside-hedenbergite series); (4) subcalcic cpx (augite); and (5) wollastonite (Wo). Table 2 lists the observed frequencies and representative Raman spectra are shown in Figure 2.

The variations of Raman frequency with Fe content (in mol%) for the opx series are in Figures 3 and 4, respectively. Augite and pigeonite show little variation in chemistry and therefore are difficult to find a systematic change in the Raman modes with respect to the iron content. For a constant Ca content, most Raman frequencies in the enstatite-ferrosilite and diopside-hedenbergite series decrease with increase iron content. We observed a linear relationship between the Raman frequencies and Fe content for all observed modes in these two series of pyroxenes. In general, the slopes ($d\nu/dx$, where x is the Fe^{2+} content in mol%) of Raman modes in the opx is steeper than those in the cpx (Table 3). All modes in opx series show negative slope except for ν_{14} and ν_{15}, which show a positive correlation with Fe^{2+} content. All modes in cpx series show

TABLE 1.—*Extended*

Mg*=Mg/(Mg+Fe)	En	Fs	Wo
0.90	0.90	0.10	0.00
0.87	0.87	0.13	0.00
0.80	0.79	0.20	0.00
0.78	0.78	0.22	0.00
0.74	0.72	0.26	0.03
0.54	0.52	0.44	0.04
0.83	0.46	0.09	0.44
0.64	0.47	0.27	0.26
0.60	0.44	0.29	0.27
0.99	0.50	0.00	0.50
0.97	0.49	0.01	0.50
0.91	0.45	0.04	0.50
0.93	0.42	0.09	0.50
0.67	0.34	0.16	0.50
0.19	0.09	0.39	0.52
1.00	0.00	0.00	1.00

TABLE 2. —*Extended*

ν_{13}	ν_{14}	ν_{15}	ν_{16}	ν_{17}	ν_{17}'	ν_{17}''
750	854	933	1013	1033	–	–
748	862	935	1006	1025	–	–
748	866	935	1007	1022	–	–
748	868	936	1004	1013	–	–
745	876	940	1003	–	–	–
747	880	942	998	–	–	–
740	884	942	994	–	–	–
–	884	946	995	–	–	–
–	888	945	993	–	–	–
–	886	946	992	–	–	–
–	884	946	991	–	–	–
–	890	949	988	–	–	–
746	857	938	1010	1025	–	–
748	858	938	1009	1025	–	–
746	860	939	1003	1019	–	–
–	860	941	1004	1019	–	–
–	864	941	1003	1014	–	–
–	880	948	997	1008	–	–
738	–	927	–	1023	1048	1060
736	–	927	–	1023	1049	1061
–	852	–	1011	–	1048	–
–	852	–	1012	–	1048	–
–	854	–	1011	–	1047	–
–	856	–	1011	–	1044	–
–	853	–	1012	–	1043	–
750	853	907	1012	–	1031	–
769*	862	–	1007	–	1038	–
–	883	970*	997	1020	1044	–

negative slope except for ν_1, ν_{14}, and ν_{15}, which show nearly flat to positive correlation with Fe^{2+} content. Accordingly, the Raman frequencies for the end-member compositions in the opx and cpx series can be obtained by the extrapolation of the linear relationships shown in Figures 3 and 4. Raman frequencies for the end-member Mg-Fe-Ca pyroxenes from the extrapolated lines in Figures 3 and 4 are listed in Table 4. The extrapolated mode frequencies of the end-members are in excellent agreement with those reported by Chopelas (1999) for enstatite (see Fig. 3) and in agreement with those of Zhang and Chopelas (unpublished data) for hedenbergite (see Fig. 4), respectively.

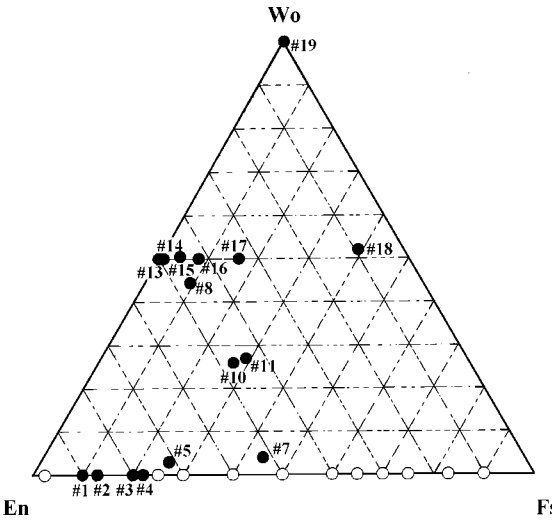

FIGURE 1. The chemical composition of the pyroxene specimens determined by the electron microprobe in this study. Solid circles = natural crystals; open circles = synthetic polycrystals.

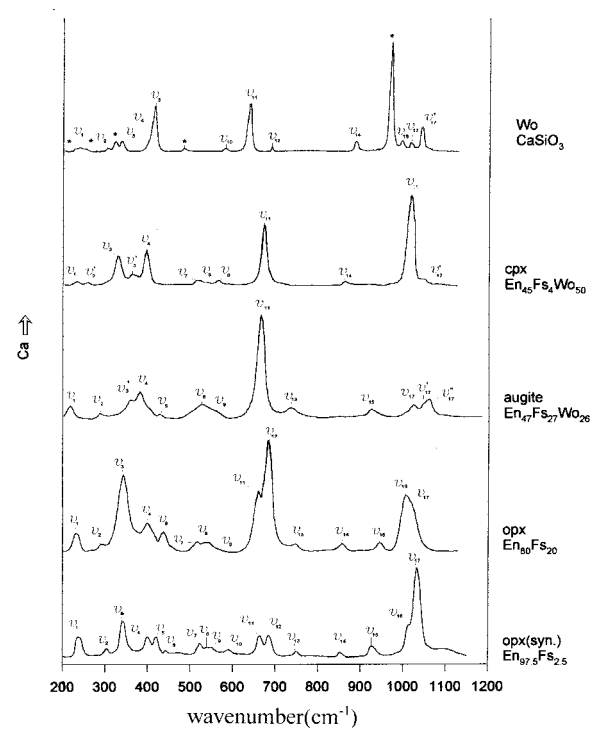

FIGURE 2. Representative Raman spectroscopic patterns of the five types of (Mg, Fe, Ca)SiO_3 pyroxenes.

DISCUSSION

Characteristic Raman-active vibrational modes of pyroxene

The Raman-active modes detected in natural and synthetic orthopyroxene specimens listed in Table 2 are designated ν_1 to ν_{17} with increasing wavenumber. Note that difference in the sym-

metry between orthopyroxene and clinopyroxene would yield spectra that are not exactly analogous. Some modes observed in the opx series will not appear in the cpx series or wollastonite. In the enstatite-ferrosilite series of the natural specimens, three moderate to weak modes (ν_1, ν_2, and ν_3) below 360 cm^{-1}, two moderate modes (ν_{11} and ν_{12}) in the range from 600 to 700 cm^{-1}, and three intense ones from 900 to 1050 cm^{-1} are the most prominent Raman vibrational modes (Fig. 2). Depending on orientation, the relative intensity of these modes may vary from run to run and may also vary with composition in this series (Fig. 13 in Lin 1995). The Raman spectra of the synthetic opx are in general similar to those of the natural samples. The synthetic samples lack ν_2 and ν_9 (except for $En_{97.5}$) but have additional ν_{10} when compared with the natural samples. Moreover, some modes such as ν_5 and ν_{17} only present in Mg-rich opx synthetic samples. The diopside-hedenbergite series differs from the opx by the appearance of four Raman modes below 360 cm^{-1}, only one mode from 600 to 700 cm^{-1} and two modes from 900 to 1050 cm^{-1}. The mode appears at ~250 cm^{-1} in the cpx series is termed ν_2' rather than ν_2 because it has a much higher frequency than ν_2 in opx. The Raman spectra of augite studied have the characteristics of both opx and cpx. However, it differs from opx by the lack of ν_{10} and ν_{12} and differs from cpx by the lack of ν_2' and the presence of ν_{15}. However, due to the limited number of the specimens examined, the result is not conclusive and may not be taken as a general character Raman modes for subcalcic cpx. The pyroxenoid wollastonite shows six modes below 360 cm^{-1} and four modes in the range between 900 to 1050 cm^{-1}, some which are drastically different from the pyroxene minerals, as indicated in Table 2. The characteristic Raman modes for the five groups of specimens in pyroxene (and pyroxenoid) are compared in Table 5.

Qualitative identification of the opx and cpx series can be achieved by checking the presence or absence of the characteristic Raman modes (Table 5). However, one should keep in mind that the absence of the Raman modes mentioned above in each series does not positively rule out the presence of the mineral in that series, only the presence of the characteristic modes in a series indicates the presence of the minerals in that series. Quantitatively, the opx and cpx can be distinguished by the frequency of ν_{14}. The frequency of ν_{14} is always greater than 854 cm^{-1} in opx while that of the cpx is less than 856 cm^{-1}.

Mode assignment

Orthopyroxene has the *Pbca* space group (D_{2h}) with Z = 8. The 240 total vibrational modes are $30A_{1g}$ (R) + $30B_{1g}$ (R) + $30B_{2g}$ (R) + $30B_{3g}$ (R) + $30A_{1u}$ + $30B_{1u}$ (IR) + $30B_{2u}$ (IR) + $30B_{3u}$ (IR) for orthoenstatite, where R and IR denote Raman- and infrared-active modes, respectively (Chopelas 1999). There are fewer the optical modes for the *C*2/*c* end-member cpx, Ca(Mg, Fe)Si_2O_6, series because Z is 4. The Raman-active modes in cpx are 14 A_g + 16 B_{lg} (Rustein and White 1971). We observed less than 20 Raman-active modes in each solid solution. From intensity considerations and compared to Chopelas (1999; Table 1) most modes are assigned as A_g. The reasons for the low number compared to theory might be that some of the modes are degenerate, some modes might be too weak to be observed, or the resolution of the present Raman spectroscopy is insufficient to identify the modes with nearly the same wavenumber. If a photomultiplier tube was used in stead of CCD as a detector, the background can be minimized and some of the weaker modes can be detected (Chopelas 1999, personal communication). A further reason may be that the disorder created by cation substitution broadens the peaks, making them indistinct. Because the symmetry differs for opx and cpx, a direct comparison of modes may be misleading. However, it is convenient to list all modes with a similar frequency together.

In general, these pyroxenes are characterized by (1) the Si-O nonbridging and bridging modes at 1020 ± 50 cm^{-1} and 900 ± 50 cm^{-1}, respectively; (2) the Si-O bending modes at 600 ± 90 cm^{-1} and (3) metal-oxygen bending and stretching modes below 600 cm^{-1}. Peaks in the 800–1100 cm^{-1} region are generally assigned to Si-O stretching vibrations, normally related to the non-bridging Si-O bonds (McMillan and Hofmeister 1988; Lazarev 1972; Farmer 1974; McMillan 1984). The wavenumber of the Si-O stretching modes of the bridging O atoms ($Si\text{-}O_{br}$) is assigned to be in the range between 650–750 cm^{-1}. The bending modes are those from the O-Si-O bends with a wavenumber between 500–590 cm^{-1}. Therefore, in the opx series, there are four modes from the stretching bridging O atoms, three modes from the stretching nonbridging O atoms, four modes from the bending O-Si-O. In addition, two modes may result from the Mg-O octahedron (375–490 cm^{-1}) and two modes from the Fe-O octahedron (225–325 cm^{-1}). The assignments are in Table 4.

Raman measurements should be carried out by inciting the polarized laser beam along some oriented crystals. The signals should be taken along some polarized directions. Mao et al. (1987) found a little variation in the wavenumber with the orientation of the crystal. In our measurements, we did not observe such phenomenon. The modes observed represent the average vibrational modes of the pyroxene in random orientation.

Variation of the Raman peaks with Fe^{2+} content

The vibrational frequency of a simple harmonic oscillator can be expressed as $\nu = 1/(2\pi)*(k/\mu)^{1/2}$ where μ is the reduced mass, k is the force constant which is assumed to be an inverse function of interatomic distance, r. The reduced mass increases with the Fe content in the pyroxene solid solutions. The negative correlation of the Raman frequency with Fe content is attributed to the increase in both reduced mass and bond length as Fe substitutes for Mg (see below).

The structure of pyroxene minerals consists of chain SiO_4 tetrahedra parallel to the *c* axis, that are linked laterally by layers containing six to eightfold-coordinated M cations. The M cations can reside in two crystallographic distinct sites, M1 and M2. M1 is nearly a regular octahedron, but the larger M2 site coordination is irregular and varies according to the atom present, sixfold for Mg, eightfold for Ca and Na. In orthorpyroxenes, long-range order occurs between divalent Mg and Fe atoms in the two M sites, with Fe preferring the larger M2 sites (Ghose 1965). In the diopside-hedenbergite series, the larger cation, Ca^{2+} predominately occupies the greater M2 sites whereas the smaller Mg^{2+} and Fe^{2+} cations are randomly distributed among the smaller M1 sites.

The average O-M1 interatomic distance of opx increases with Fe content (Domenegheti et al. 1985). A similar trend also

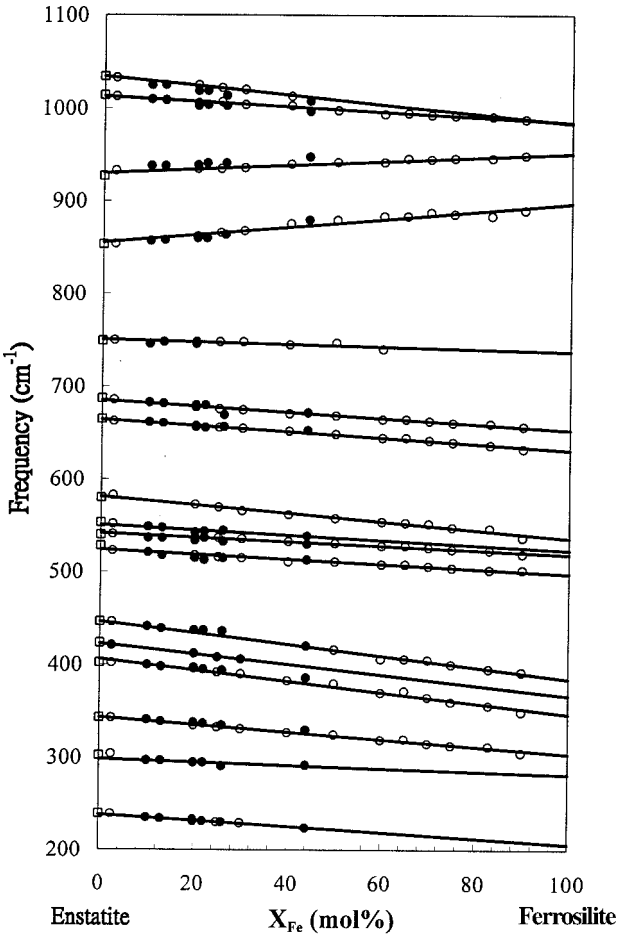

FIGURE 3. Raman frequencies vs. Fe content for the enstatite-ferrosilite series. Solid circles = natural crystals; open circles = synthetic polycrystals. Data of enstatite reported by Chopelas (1999) are shown as open squares.

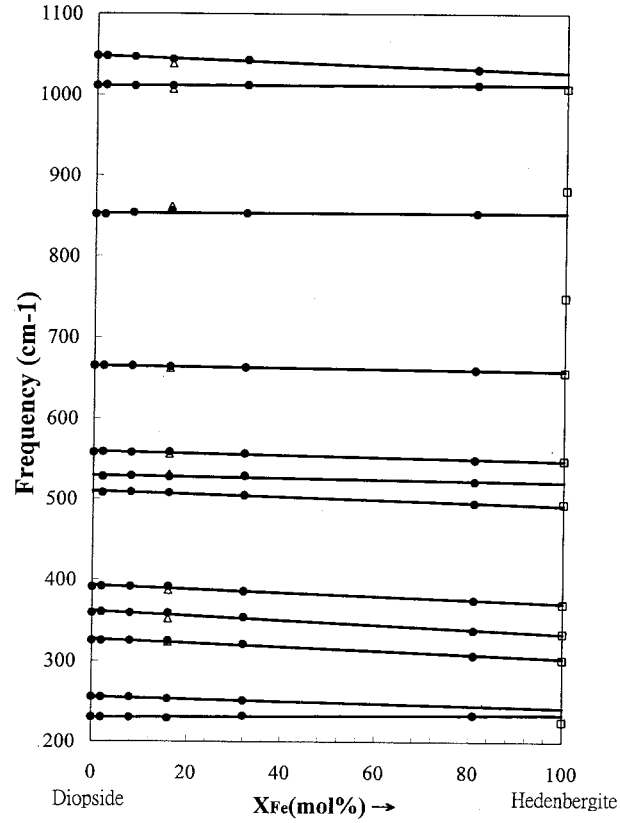

FIGURE 4. Raman frequencies vs. Fe content for the diopside-hedenbergite series. Solid circles: composition with Wo = 50 mol%. Open triangles = composition with Wo = 44 mol% (no. 8, Table 2). Open squares = unpublished data from Zhang and Chopelas.

TABLE 3. The slope of Raman frequency versus composition (dv/dx) for various modes in the opx and cpx series

	Enstatite–ferrosilite series	Diopside–hedenbergite series
ν_1	–0.3196	+0.0423
ν_2'	–	–0.1339
ν_2	–0.1684	–
ν_3	–0.4018	–0.2296
ν_3'	–	–0.273
ν_4	–0.6097	–0.216
ν_5	–0.5542	–
ν_6	–0.6223	–
ν_7	–0.2388	–0.179; –0.828
ν_8	–0.2457	–
ν_9	–0.2777	–0.1189
ν_{10}	–0.461	–
ν_{11}	–0.3308	–0.0639
ν_{12}	–0.3114	–
ν_{13}	–0.143	–
ν_{14}	+0.4067	+0.0016
ν_{15}	+0.1916	+0.0097
ν_{16}	–0.2792	–
ν_{17}	–0.5234	–
ν_{18}	–	–0.2098

exists for M2. Therefore, most of the vibrational modes in opx decrease in wavenumber as Fe content increases. However, for the cpx series substitution of Fe for Mg does not cause a serious distortion in the octahedron and, therefore, does not cause a significant variation in the Raman frequency as compared with opx series. The relatively rigid Si-O bands can be affected by the cation substitution. The frequency of the ν_1 mode of cpx shows a positive correlation with the Fe content and cannot be accounted for by the mechanism proposed above. However, if 225 cm^{-1} (from Zhang and Chopelas 1994) is taken as the ν_1 mode frequency of the end-member hedenbergite, then a negative slope is established. However, in both of the opx and cpx series, some other modes show a positive dv/dx slope which needs to be accounted for.

In pyroxene, the interatomic distance of Si-O_{br} decreases as the mean ionic radius of the cation increases while the interatomic distance of Si-O_{nbr} increases as the mean ionic radius of cation increases (Cameron and Papike 1981; Domeneghetti et al. 1985). The mean ionic radius of the M-cation increases with Fe^{2+} substitution for magnesium in pyroxenes. Therefore, the modes of which the frequency shows positive correlation with the Fe content may be related to the stretching between the bridg-

TABLE 4. Raman modes of the end-member Mg-Fe-Ca pyroxenes

	Enstatite	Fesilite	Diopside	Hedenbergite	Wollastonite	Mode type
ν_1	238	206	230	234	226	M-O stretch
ν_2'	–	–	255	242	237, 337	Ca-O stretch
ν_2	298	281	–	–	–	Mg-O stretch
ν_3	344	304	327	304	303	M-O stretch
ν_3'	–	–	360	333	321, 337	Ca-O stretch
ν_4	407	346	393	372	–	Mg-O stretch
	–	–	–	–	400, 412	Ca-O stretch
ν_5	422	367	–	–	–	Mg-O stretch
ν_6	447	685	–	–	–	Mg-O stretch
ν_7	522	498	510, 530	492, 521	485	O-Si-O bend
ν_8	543	518	–	–	-—	O-Si-O bend
ν_9	551	523	559	547	–	O-Si-O bend
ν_{10}	582	536	–	–	581	O-Si-O bend
ν_{11}	665	632	665	659	636	Si-O-Si bend
ν_{12}	685	653	–	–	688	Si-O-Si bend
ν_{13}	751	737	–	–	–	Si-O-Si bend
ν_{14}	856	897	853	855	883	Si-O(br) stretch
ν_{15}	931	950	1010	1012	970	Si-O(br) stretch
ν_{16}	1013	985	–	–	997	Si-O(br) stretch
ν_{17}	1035	983	–	–	1020	Si-O(br) stretch
ν_{17}'	–		1047	1027	1044	Si-O(br) stretch

TABLE 5. Characteristic Raman modes of the five groups of specimens in pyroxene

	200–360 cm^{-1}	900–1050 cm^{-1}	ν_2'	ν_2	ν_6	ν_9	ν_{10}	ν_{12}	ν_{15}	ν_{14}
synthetic opx	2–3 modes	2–3 modes	–	+	±	±	+	+	+	>854
natural opx	3 modes	3 modes	–	+	+	+	–	+	+	>854
cpx	4 modes	2 modes	+	–	–	+	–	–	–	<856
augite	2 modes	4 modes	–	+	–	+	–	–	+	–
Wo	6 modes	4 modes	+	+	+	+	+	–	+	883

ing oxygen and silicon because the Si-O_{br} distance decreases with an increase in the Fe content. According to this interpretation, the Si-O_{br} stretching mode frequencies are less than those for the Si-O_{nbr} modes in the opx series, which is contrary to Williams' (1995) scheme. Moreover, the Si-O_{nbr} mode frequencies generally decrease with the Fe content in Mg-Fe silicate solid solution such as the forsterite to fayalite series where there are no bridging bonds (e.g., Guyot et al. 1986).

RAMAN SPECTROSCOPY AS A MICROPROBE FOR PYROXENES

Based on Raman peak positions, the major-element composition of the (Mg, Fe, Ca)-pyroxenes can be estimated. The benefit of using Raman as a tool for chemical identification of minerals is its nondestructive nature, and the sample size under investigation can be as small as a few micrometers.

The Raman modes showing the greatest variation in frequency with the Fe^{2+} content are potentially capable of being used as an index for determining the Fe content in the opx and cpx series. The best Raman modes for this purpose in the opx series are ν_6 (447–385 cm^{-1}) and ν_{14} (856–897 cm^{-1}) pairs that show about 60 cm^{-1} across the series. The ν_{15} (931–950 cm^{-1}) mode can also serve as a supplementary mode for the determination of the composition. These modes are characteristic and fairly intense. However, in the cpx series, because only the ν_3 (327–304 cm^{-1}) and ν_3' (360–333 cm^{-1}) pairs show a variation more than 20 cm^{-1}. These provide a weaker basis for the composition indices. The uncertainties in the determination of the Fe content with the Raman modes are of the order of 3 and 6% in the opx and cpx series, respectively.

The cpx series plotted on Figure 4 showing linear relationship of mode frequencies vs. Fe content have Wo contents near 50 mol%. Raman mode frequencies of cpx with a large amount of Ca content would yield a recognizable difference from the linear trends shown in Figure 4. For instance, cpx with the composition of $En_{0.46}Fs_{0.09}WO_{0.44}$ has it Raman mode frequencies deviate from the linear trends and can be resolved by the Raman spectroscopy.

ACKNOWLEDGMENTS

We thank H.K. Mao for providing synthetic samples of orthopyroxene and helpful comments during the preparation of this manuscript. We acknowledge the help from V. Cheng for the preparation of the diagrams. This is a publication of the Institute of Earth Sciences, Academia Sinica.

REFERENCES CITED

Calas, G. and Hawthorne, F.C. (1988) Introduction to spectroscopic methods. In Mineralogical Society of America Reviews in Mineralogy, 18, 1–9.

Cameron, M. and Papike, J.J. (1981) Structural and chemical variations in pyroxenes. American Mineralogist, 66, 1–50.

Chen, C.H., Presnell, D.C., and Stern, R.J. (1992) Petrogenesis of ultramafic xenoliths from the 1800 Kaupulehu flow, Hualalai Volcano, Hawaii. Journal of Petrology, 33, 163–202.

Chopelas, A. (1999) Estimates of mantle relevant Clapeyron slopes in the $MgSiO_3$ system from high-pressure spectroscopic data. American Mineralogist, 84, 233–244.

Deer, W.A., Howie, R.A., and Zussman, J. (1966) Introduction to the Rock Forming Minerals. Wiley, New York.

Domeneghetti, M.C., Molin, G.M., and Tazzoli, V. (1985) Crystal-chemical implications of the Mg^{2+}-Fe^{2+} distribution in orthopyroxenes. American Mineralogist, 69, 987–995.

Farmer, V.C. (1974) Orthosilicate, pyrosilicates, and other finite-chain silicates. In V.C. Farmer, Ed., The Infrared Spectra of Minerals, p. 285–303. Mineralogical Society of London.

Ghose, S. (1965) Fe^{2+}-Mg^{2+} order in an orthopyroxene. Zeitschrift für Kristallographie, 122, 81–99.

Ghose, S., Choudhury, N., Chaplot, S.L., Pal Chowdhury, C., and Sharma, S.K. (1994) Lattice dynamics and Raman spectroscopy of protoenstatite $Mg_2Si_2O_6$. Physics of Chemistry and Minerals, 20, 469–477.

Guyot, F., Boyer, H., Madon, M., Velde, B., and Poirier, J.P. (1986) Comparison of the Raman microprobe spectra of $(Mg,Fe)_2SiO_4$ and Mg_2GeO_4 with olivine and spinel structures. Physics of Chemistry and Minerals, 13, 91–95.

Jarosewich, E., Nelsen, J.A., and Norberg, J.A. (1980) Reference samples for electron microprobe analysis, Geostand. Newsletter, 4, 43–48.

Kieffer, S.W. (1985) Heat capacity and entropy: systematic relations to the lattice vibrations. In Mineralogical Society of America Reviews in Mineralogy, 14, 65–126.

Lazarev, A.N. (1972) Vibrational Spectra and Structure of Silicates. Translated by G.D. Archard, trans. editor V.C. Farmer, Consultants Bureau, New York, 302 p. (in Russian)

Lin, I.H. (1995) Raman Spectroscopy study of (Ca, Mg, Fe)-Pyroxene. Master Thesis, National Taiwan University, 74 p.

McMillan, P. (1984) Structural studies of silicate glasses and melts: applications and limitations of Raman spectroscopy. American Mineralogist, 69, 633–644.

McMillan, P.F. and Hofmelster, A.M. (1988) Infrared and Raman spectroscopy. In Mineralogical Society of America Reviews in Mineralogy, 18, 99–159.

Mao, H.K., Hemley, R.J., and Chao, E.C.T. (1987) The application of micro-Raman spectroscopy to analysis and identification of minerals in thin section. Scanning Microscopy, 1, 495–501.

Rutstein, M.S. and White, W.B. (1971) Vibrational spectra of high-calcium pyroxenes and pyroxenoids. American Mineralogist, 56, 877–887.

Wang, A., Han, J., Guo, L., Yu, J., and Zeng, P. (1994) Database of standard Raman spectra of minerals and related inorganic crystals. Applied Spectroscopy, 48, 959–968.

White, W.B. (1975) Structural interpretation of lunar and terrestrial minerals by Raman spectroscopy. In C. Karr, Jr., Ed., Infrared and Raman Spectroscopy of Lunar and Terrestrial Minerals, p. 325–358. Academic Press, New York.

Williams, Q. (1995) Infrared, Raman and optical spectroscopy of Earth materials. In T.J. Ahrens, Ed., Mineral Physics and Crystallography: A Handbook of Physical Constants, p. 291–302. American Geophysical Union, Washington, D.C.

Xu, J., Huang, E., Lin, J.F., and Xu, L.Y. (1995) Raman study at high pressure and the thermodynamic properties of corundum: Application of Kieffer's model. American Mineralogist, 80, 1157–1165.

Yang, H. and S. Ghose (1994) Thermal expansion, Debye temperature and Gruneisen parameter of synthetic $(Fe,Mg)SiO_3$ orthopyroxenes. Physics of Chemistry and Minerals, 20, 575–586.

MANUSCRIPT RECEIVED SEPTEMBER 29, 1998
MANUSCRIPT ACCEPTED NOVEMBER 16, 1999
PAPER HANDLED BY ANASTASIA CHOPELAS